J Nanostruct 16(2): 1657-1666, Spring 2026

RESEARCH PAPER

Effect of Boron Doping on the Fabrication and Characterization of Zinc Oxide Nanoparticle Thin Films Deposited Using Spray Pyrolysis Technique

Manal Dakhil Sakhil

Faculty of Physical Education and Sports Sciences, University of Kerbala, Iraq

ARTICLE INFO

Article History:
Received 28 November 2025
Accepted 21 February 2026
Published 01 April 2026

Keywords:
Boron
Spray Pyrolysis Technique
Structural and optical properties
Zinc oxide NP

ABSTRACT

Two different amounts of boron, 2% and 4%, were added to zinc oxide (ZnO) films using the spray pyrolysis technique (SPT), in addition to un-doped ZnO films. Grain size increased from 11.14 nm to 12.29 nm as boron was added and its quantities were increased, according to structural research, indicating that the sample films are polycrystalline. According to the results of the X-ray diffraction analysis, the major crystallographic reflection is the (101) plane. The deposited film samples were examined using Atomic Force Microscopy (AFM). Nanostructured ZnO films with 0% doping, 1% boron doped, and 4% boron doped had average particle sizes of around 78.70 nm, 67.78 nm, and 42.10 nm, respectively. Undoped ZnO had a root mean square roughness (Rrms) of 9.68 nm, whereas boron-doped ZnO had a Ra value of 4.79 nm and a Ra value of 3.34 nm. A visible-light transmittance of more than 65% was achieved. Optical bandgap values also decreased following boron addition, from 3.16 eV to 3.04 eV. Additionally, the dopant concentration rose in tandem with the absorption coefficient, especially once the boron level hit 3%. The results also showed that the refractive index and extinction coefficient improved as the boron level rose.

How to cite this article
Sakhil M. Effect of Boron Doping on the Fabrication and Characterization of Zinc Oxide Nanoparticle Thin Films Deposited Using Spray Pyrolysis Technique. J Nanostruct, 2026; 16(2):1657-1666. DOI: 10.22052/JNS.2026.02.018

INTRODUCTION

As an earth element, boron (b) is not common. Metals are unique among elements due to their characteristics, such as their low brittleness and great hardness. Ceramics, metal alloys, and industrial plastic fibers are the main products that use boron as an insulator and reinforcement agent [1]. Metal oxides doped with boron have unique qualities that impact carrier mobility. These properties include a stable B3+ state, a high Lewis acid strength of 10.709, a strong dissociation energy of 8008.8 kJ mol^{-1}, and a high energy required for the production of an oxygen vacancy of 8.374 eV. Based on the inherent bond strength and dissociation energy, boron (B) can be used as a dopant to improve metal (M) and oxygen (O) lattice sites. [2]. The use of SPT technology to create ZnO films has garnered considerable attention throughout the past ten years. Zinc oxide has sparked widespread interest because to its straight broad bandgap of 3.31 eV and hexagonal wurtzite structure [3]. The use of ZnO as TCO to replace conventional indium tin oxide in solar cells is a hot topic [4]. The insertion of boron

* *Corresponding Author Email: manal.dakhil@uokerbala.edu.iq*

(B) dopants into ZnO has been shown to disrupt the crystal structure. Nonetheless, an optimization procedure resulted in an improvement in c-axis-oriented crystal formation. [5]. The use of ZnO as TCO to replace traditional indium tin oxide in solar cells is one area of great interest. ZnO has gained importance in many applications, including solar cells, anti-reflective coating gas sensors, LED, heat mirrors, and SAWD [3–6]. It can be fabricated in many techniques like Sputtering [7], MBE [8], PLD [9], CVD [10], SPT [11, 12], and sol-gel [13, 14]. The provided text discusses the impact of boron (B) doping on various characteristics of zinc oxide (ZnO) films. The studies, particularly one by T. Hurma, focused on how introducing boron into ZnO films affects their the optical, structural, and electrical characteristics. the Crystallization and Concentration of B Doping: T. Hurma's study demonstrated Considering the boron concentration doping increased in ZnO sheets, the degree of crystallization decreased. To put it differently, elevated levels of boron doping caused a decline in the overall crystalline quality of the ZnO films. This phenomenon might stem from the disruptive influence of boron atoms within the regular zinc oxide lattice, introducing defects or distortions into the crystalline arrangement. Regarding surface roughness and boron doping, an increase in boron doping concentration resulted in rougher surfaces for the ZnO films. One possible explanation for the rise in surface roughness is the unequal boron atom integration that occurs throughout the film's development [15]. For this study, the ZnO thin films were synthesized using the chemical spray pyrolysis technique. This research delves into the interplay between boron doping and ZnO thin films by examining its effects on their optical characteristics and nanostructure.

MATERIALS AND METHODS

Thin ZnO and ZnO: B films were fabricated using the Chemical Spray Pyrolysis technique. The matrix solution was prepared by diluting aqueous 0.05 M zinc hydrate ($Zn(CH_3COO)_2.2H_2O$) from BDH Chemicals, England, in 100 mL of deionized water. For doping, Boron at 0.1M concentration ($B(NO_3)_2.3H_2O$) was dissolved in deionized water to create 2% and 4% volumetric ratios. During deposition, the substrate temperature was set to 450°C. Nitrogen (N^2) served as the carrier gas, and the separation between the nozzle along with maintaining the base at 29 cm. The spraying process involved a 9-second spraying duration, an average spraying rate of 5 mL/min, and a 2-minute interval between successive spray applications. The gravimetric method determined the film thickness, yielding a measurement of around 300±25 nm. Structural properties were analyzed through X-ray diffraction (XRD) utilizing a Shimadzu XRD-6000 instrument from Japan. Surface morphology was investigated using an Atomic Force Microscope (AFM), specifically the AA 3000 Scanning Probe Microscope, also from Japan. Transmittance evaluation was executed using a spectrophotometer, specifically the Shimadzu UV-probe 1640, originating from Japan.

RESULTS AND DISCUSSIONS

The X-ray diffraction (XRD) patterns of the grown films are depicted in Fig. 1. These spectra clearly indicate due to the films' polycrystalline nature, showcasing three primary peaks that correspond to the (100), (101), (102), and (103) planes at 31.71°, 36.62°, 47.51°, and 62.76°, respectively. The peak at 36.62° corresponds to the (101) plane and conforms to a value of 36.62° (ICDD No. 36-1451) [16].

The crystallite size (D) of the films is determined using Scherrer's equation [17, 18]:

$$D = \frac{0.9\lambda}{\beta\cos\theta} \quad (1)$$

θ, the incidence wavelength (λ), and FWHM (Full Width at Half Maximum) are described here. D value decreased from 11.14 nm to 12.29 nm when boron doping into ZnO increased. In order to calculate the dislocation density (δ), a formula is utilized. [19, 20]:

$$\delta = \frac{1}{D^2} \quad (2)$$

The lattice strain (ε) was calculated using the tangent formula [21, 22]:

$$\varepsilon = \frac{\beta\cos\theta}{4\pi} \quad (3)$$

With increased boron doping, both calculated dislocation density values and strain displayed an upward trend [23]. The interplay between D, lattice parameters, and boron content was explored, and the results are presented in Table 1. The relationship between FWHM, D, and boron content is shown in Fig. 2. Notably, the structural

parameters S_p and D exhibit an inverse relationship.

The AFM images presented in Fig. 3 offer a visual representation of the deposited films, while Table 2 provides quantitative data in terms of average roughness (Ra) or root mean square (Rrms) for these films. The images depict films that are uniformly distributed in microscale granules, exhibiting a seamless distribution without noticeable gaps between them, as evident in Fig. 3 (a_3, b_3, and c_3). The calculated average particle size (Pav) for the nanostructured ZnO films falls within the range of approximately 78.70 nm, 67.78 nm, and 42.10 nm for un doped ZnO, ZnO doped with 2% boron, and ZnO doped with 4% boron, respectively. This indicates a systematic decrease in particle size with increasing boron doping concentration. The Ra values for un doped ZnO and ZnO doped with boron are measured as 9.68 nm, 4.79 nm, and 3.34 nm, respectively, while the Rrms values are 11. These values signify that the surface roughness decreases with boron doping, suggesting a smoothing effect on the film surfaces. Furthermore, the data suggests a clear impact of boron content on both Ra and Rrms, demonstrating the influence of boron doping concentration on the surface characteristics of the ZnO films. The detailed values of AFM parameters (PAFM) can be found in Table 2, providing a comprehensive overview of the surface morphology and roughness for each film.

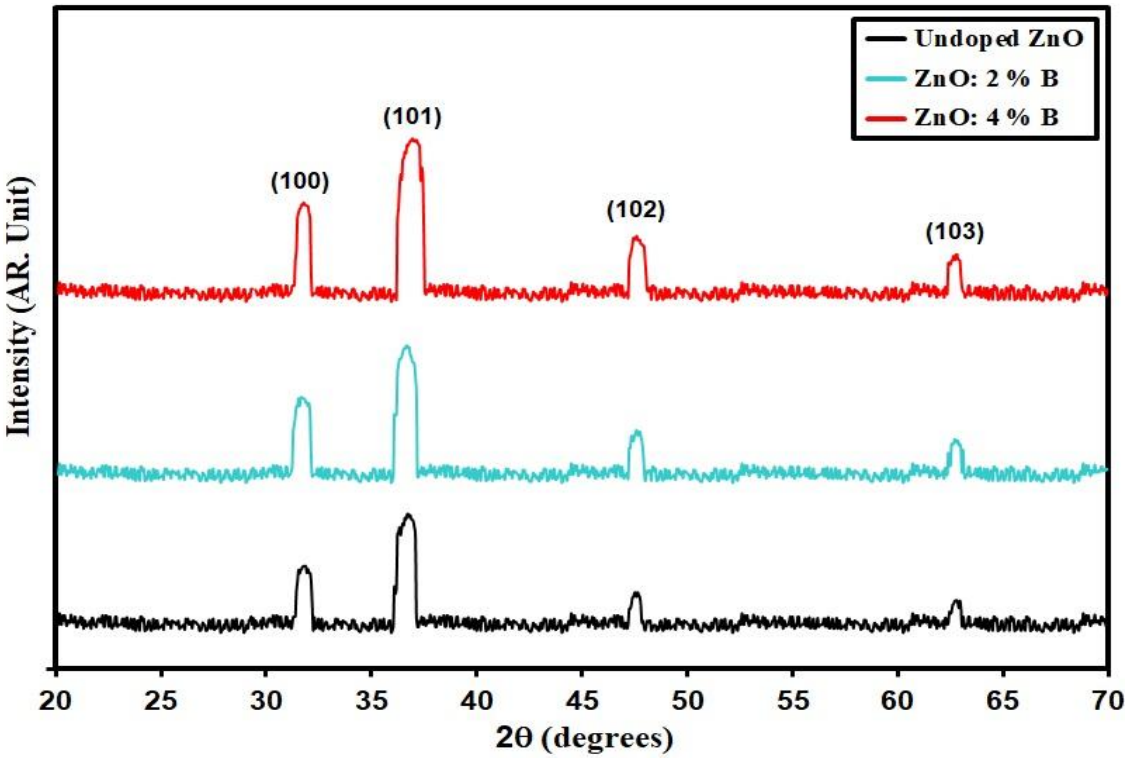

Fig. 1. Illustrates the fabricated films' X-ray diffraction (XRD) patterns.

Table 1. Presents the values of D (crystallite size) and Sp (optical bandgap) for the studied films.

Sample	2? (°)	(hkl) Plane	FWHM (°)	E_g (eV)	*D* (nm)	δ(× 10^{14}) (lines/m^2)	ε (× 10^{-4})
Un doped ZnO	36.22	101	0.75	3.16	11.14	80.58	31.09
ZnO: 2% B	3.18	101	0.72	3.10	11.61	74.18	29.85
ZnO: 4% B	36.15	101	0.68	3.04	12.29	66.20	28.20

Through measuring their transmittance in the UV-Vis range of 300 to 900 nm, the films' optical properties were investigated. A typical way to communicate experimental results is as a percentage transmittance, or T, which is defined as [24, 25]:

$$T\% = \frac{I}{I_o}\% \quad (4)$$

Io represents the beginning light intensity and (I) represents the light intensity after passing through the sample.

Pictured in Fig. 4 are the corresponding film transmittance values. Surprisingly, the visible spectrum has a transmittance of above 65%. Transmittance increased with decreasing dopant concentration, particularly at boron concentrations up to 3%. The absorption that impurities cause might account for this pattern, as their ionization energies are close to the energy gap of the incoming photons. [26, 27].

The film's measured absorbance (A) is connected to its transmittance (T) by means of the

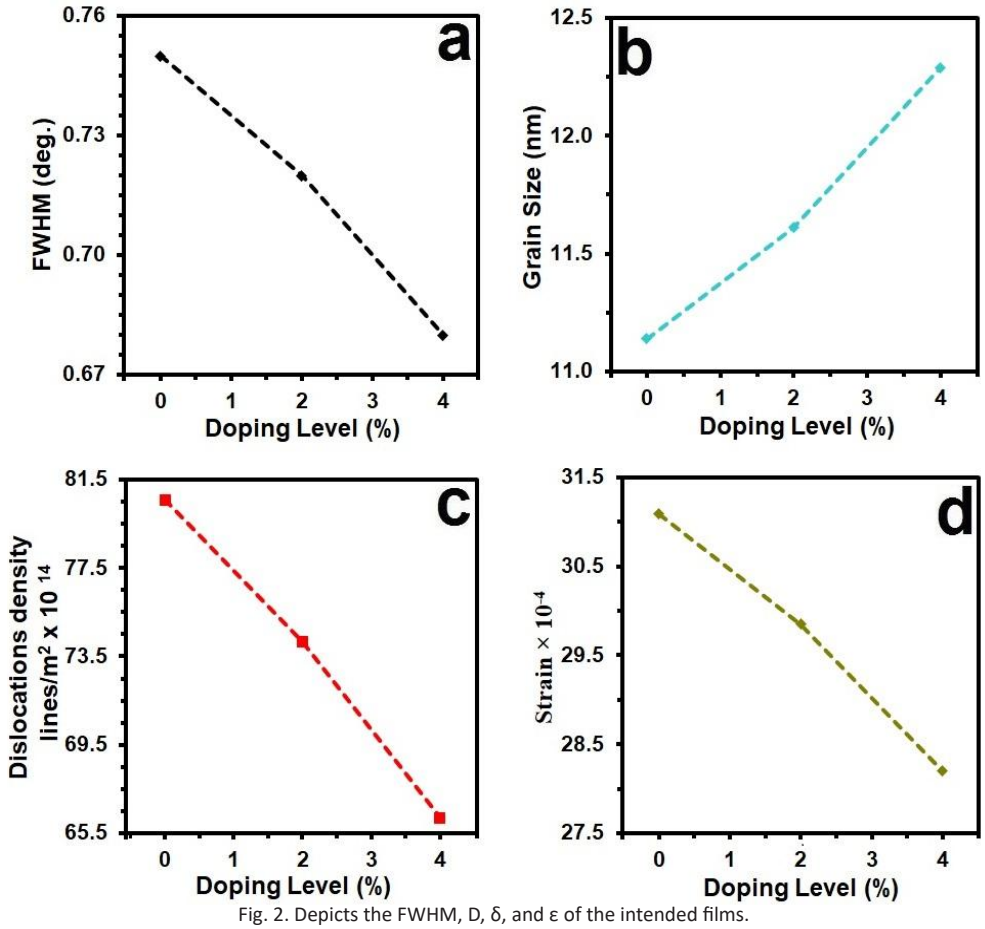

Fig. 2. Depicts the FWHM, D, δ, and ε of the intended films.

Table 2. Presents the values of PAFM (parameters obtained from AFM analysis) for the targeted films.

Samples	P_{av} nm	R_a (nm)	R. M. S. (nm)
Un doped ZnO	78.70	9.68	11.56
ZnO: 2% B	67.78	4.79	10.45
ZnO: 4% B	42.10	3.32	3.34

Eq. 5: [28, 29]:

$$A = \log\left(\frac{1}{T}\right) = \left(\frac{I}{I_o}\right) \quad (5)$$

in where (I) is the amount of light that escapes the system and (Io) is the amount of light that enters it. The absorption and transition spectra of thin films of B-doped ZnO are shown in Fig. 5. One thing that stands out from these spectra is that the absorbance values for transitions go lower as the amount of Boron gets higher. It may be deduced that indium doping resulted in greater optical density in ZnO films since the transition level represents optical density [27].

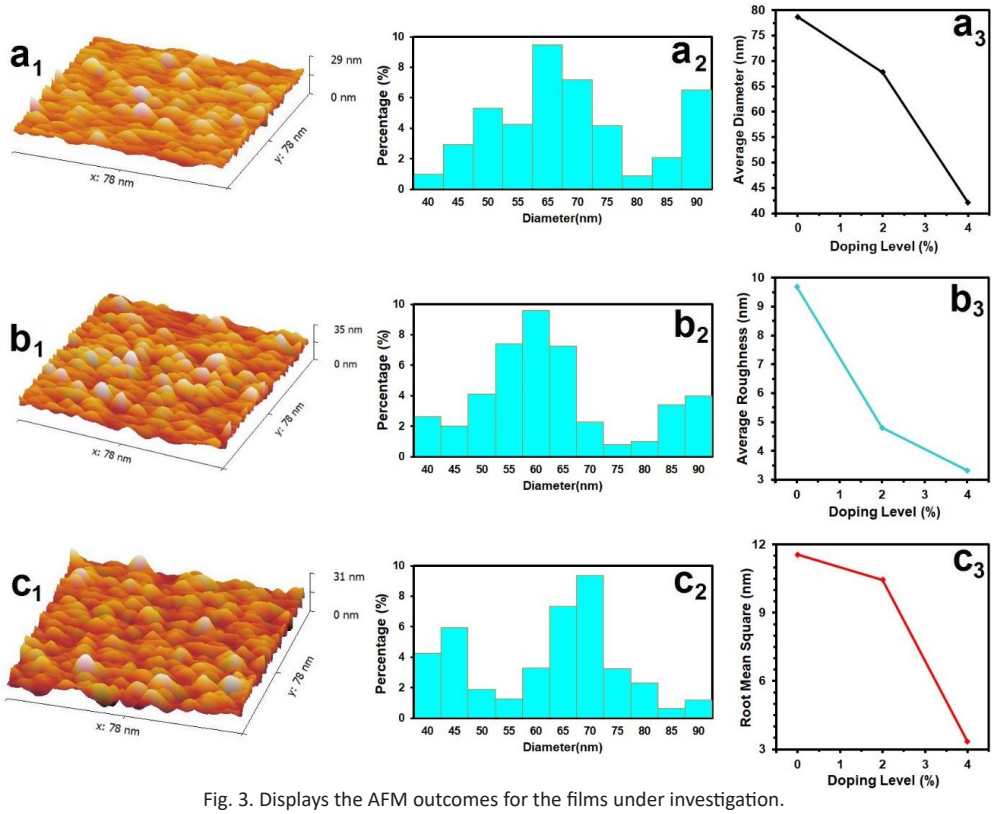

Fig. 3. Displays the AFM outcomes for the films under investigation.

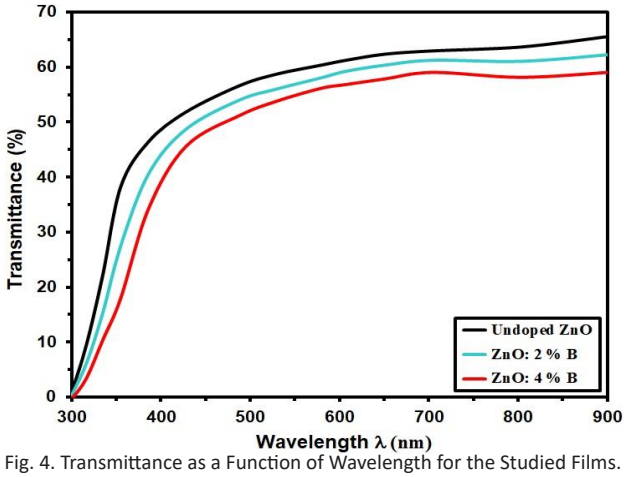

Fig. 4. Transmittance as a Function of Wavelength for the Studied Films.

The absorption coefficient (α) is determined using Eq. 6 [20, 31]:

$$\alpha = \frac{\ln (1/T)}{d} \quad (6)$$

where d represents the film thickness. Fig. 6 illustrates the relationship between the absorption coefficient (α) and the studied films. It is evident that the absorption coefficient increases as the dopant concentration rises, particularly up to 4% of the boron content. This observation suggests that the transition is likely associated with a direct electronic transition, and the characteristics of this state are crucial as they contribute to electrical conduction [32].

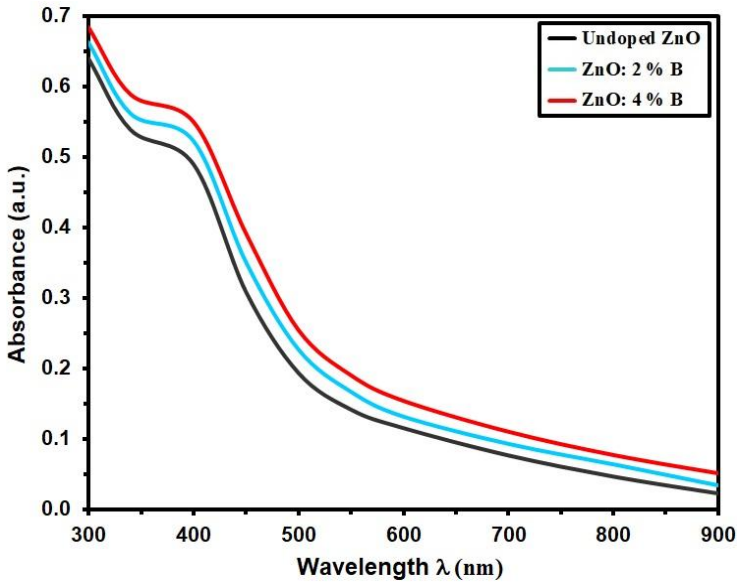

Fig. 5. Absorption of Pure and ZnO:B Films at Different Dopant Levels.

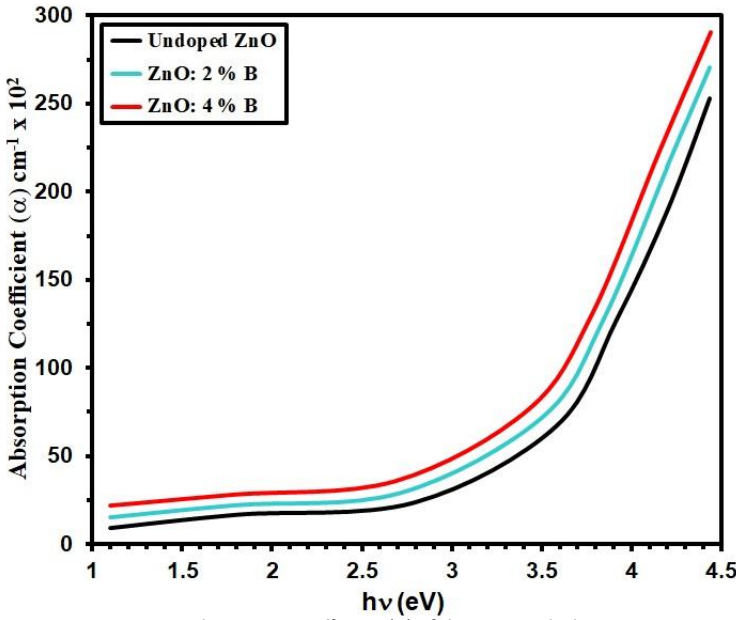

Fig. 6. Absorption Coefficient (α) of the Prepared Films.

The bandgap energy E_g is determined using Tauc's relation [33,34]:

$$\alpha h\nu = A(h\nu - E_g)^{\frac{1}{2}} \quad (7)$$

where A is a constant. From Fig. 7, it can be deduced that the bandgap of un doped ZnO is influenced by the boron content, and as the doping concentration increases E_g decreases. Specifically, the bandgap values for the synthesized nanocrystalline un doped ZnO and ZnO doped with 4% boron thin films are measured as 3.16 eV and 3.04 eV, respectively. which is due to the increased crystallization increasing the particle size and reducing the areas of defects in the grid [35].

To determine the extinction coefficient (k), the following relation was utilized [35, 36]:

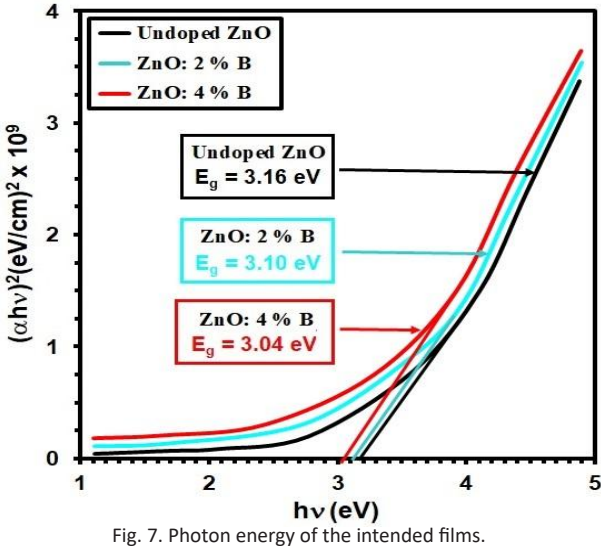

Fig. 7. Photon energy of the intended films.

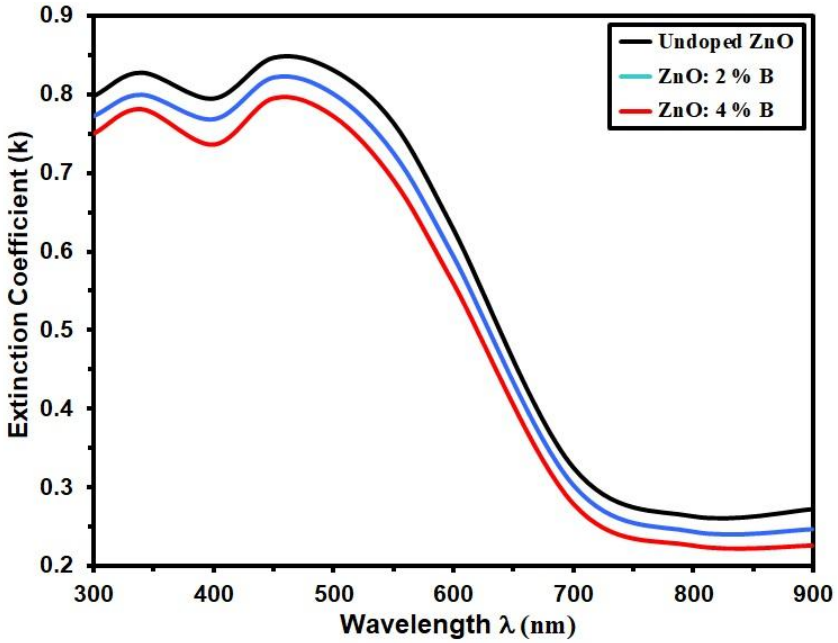

Fig. 8. Extinction coefficient of the intended films.

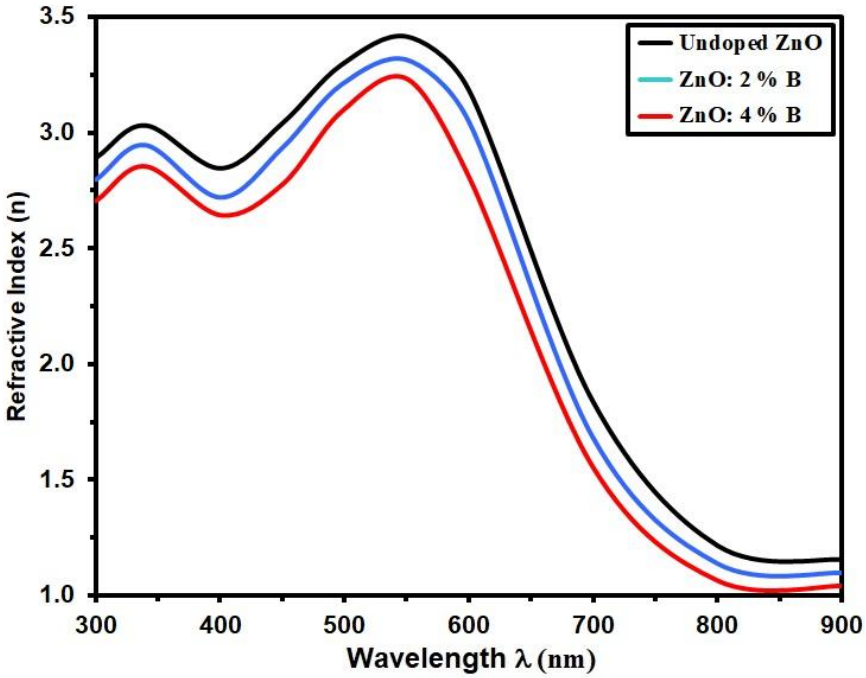

Fig. 9. Refractive index of intended films.

$$k = \frac{\alpha\lambda}{4\pi} \quad (8)$$

Where λ is the wavelength. Fig. 7 presents the variation of the extinction coefficient of chiaund oped ZnO and ZnO:B films in relation to the wavelength. Fig. 8 demonstrates that K increases with the augmentation of boron content [15].

Utilizing the reflectance (R) spectra serve as a means to Establish the refractive index (n) [37, 38]:

$$R = \left(\frac{n-1}{n+1}\right)^2 \quad (9)$$

To determine n, the following formula was utilized [39, 40]:

$$n = \frac{1+\sqrt{R}}{1-\sqrt{R}} \quad (10)$$

Fig. 9 depicts the relationship between n and λ variations. The refractive index spectra of all films showed a similar pattern of activity. After increasing the dopant concentration up to 4 percent of the Boron content in the films, there is a slight drop in the refractive index values of the films [41].

CONCLUSION

The synthesis of ZnO and ZnO.B films on glass substrates has been conducted. The results indicate that the inclusion of boron in the structure significantly affects the attributes examined. The XRD signals of the produced films validate their polycrystalline characteristics. Notably, the average dislocation density values were found to escalate with increasing boron doping content. The surface topography of the produced films decreases as the boron content in the film rises. In line with this, the transmittance within the visible range surpasses 65% as the boron content increases. The absorption coefficient experiences a slight increase, while the refractive index and extinction coefficient exhibit a decrease. Furthermore, the optical bandgap of un doped ZnO and ZnO doped with Boron (ZnO:B) films, pertaining to direct allowed transitions, has been reduced from 3.16 eV to 3.04 eV.

CONFLICT OF INTEREST

The authors declare that there is no conflict of interests regarding the publication of this

manuscript.

REFERENCES

1. Schurink B, van den Beld WTE, Tiggelaar RM, van de Kruijs RWE, Bijkerk F. Synthesis and Characterization of Boron Thin Films Using Chemical and Physical Vapor Depositions. Coatings. 2022;12(5):685.
2. Shankar P, Srinivasan P, Vutukuri B, Kulandaisamy AJ, Mani GK, Babu KJ, et al. Boron induced c-axis growth and ammonia sensing signatures of spray pyrolysis deposited ZnO thin films – Relation between crystallinity and sensing. Thin Solid Films. 2022;746:139126.
3. Xingwen Z, Yongqiang L, Ye L, Yingwei L, Yiben X. Study on ZnO thin films deposited on sol–gel grown ZnO buffer by RF magnetron sputtering. Vacuum. 2006;81(4):502-506.
4. Kumar J, Attridge A, Wood PKC, Williams MA. Analysis of the effect of cone-beam geometry and test object configuration on the measurement accuracy of a computed tomography scanner used for dimensional measurement. Meas Sci Technol. 2011;22(3):035105.
5. Sharma S, Tran A, Nalamasu O, Dutta PS. Spin-coated ZnO thin films using ZnO nano-colloid. J Electron Mater. 2006;35(6):1237-1240.
6. Minami T, Nanto H, Takata S. Highly conductive and transparent ZnO thin films prepared by r.f. magnetron sputtering in an applied external d.c. magnetic field. Thin Solid Films. 1985;124(1):43-47.
7. Li BS, Liu YC, Chu ZS, Shen DZ, Lu YM, Zhang JY, et al. High quality ZnO thin films grown by plasma enhanced chemical vapor deposition. J Appl Phys. 2002;91(1):501-505.
8. Mandalapu LJ, Xiu F, Yang Z, Liu J. UV photoconductors based on Ga-doped ZnO films. MRS Proceedings. 2005;891.
9. Hu WS, Liu ZG, Guo XL, Lin C, Zhu SN, Feng D. Preparation of c-axis oriented ZnO optical waveguiding films on fused silica by pulsed laser reactive ablation. Mater Lett. 1995;25(1-2):5-8.
10. Realization and Characterization of ZnO/n-Si Solar Cells by Spray Pyrolysis. Egyptian Journal of Solids. 2005;28(2):243-254.
11. Hassan ES, Mubarak TH, Chiad SS, Habubi NF, Khadayeir AA, Dawood MO, et al. Physical Properties of indium doped Cadmium sulfide thin films prepared by (SPT). Journal of Physics: Conference Series. 2019;1294(2):022008.
12. Schuler T, Aegerter MA. Optical, electrical and structural properties of sol gel ZnO:Al coatings. Thin Solid Films. 1999;351(1-2):125-131.
13. Mursal, Irhamni, Bukhari, Jalil Z. Structural and Optical Properties of Zinc Oxide (ZnO) based Thin Films Deposited by Sol-Gel Spin Coating Method. Journal of Physics: Conference Series. 2018;1116:032020.
14. Jasim SA, Banimuslem HAJ, Alsultany FH, Al-Bermany E, Mohammed RM. Ammonia and nitrogen dioxide detection using ZnO/CNT nanocomposite synthesized by sol–gel technique. J Sol-Gel Sci Technol. 2023;108(3):734-741.
15. Hurma T. Effect of boron doping concentration on structural optical electrical properties of nanostructured ZnO films. J Mol Struct. 2019;1189:1-7.
16. Bose S, Barua AK. The role of ZnO:Al films in the performance of amorphous-silicon based tandem solar cells. J Phys D: Appl Phys. 1999;32(3):213-218.
17. Alawi AI, Al-Bermany E. Newly Fabricated Ternary PAAm-PVA-PVP Blend Polymer Doped by SiO_2: Absorption and Dielectric Characteristics for Solar Cell Applications and Antibacterial Activity. Silicon. 2023;15(13):5773-5789.
18. Jandow NN, Othman MS, Habubi NF, Chiad SS, Mishjil KA, Al-Baidhany IA. Theoretical and experimental investigation of structural and optical properties of lithium doped cadmium oxide thin films. Materials Research Express. 2019;6(11):116434.
19. Hassan ES, Qader KY, Hadi EH, Chiad SS, Habubi NF, Abass KH. Sensitivity of Nanostructured Mn-Doped Cobalt Oxide Films for Gas Sensor Application. Nano Biomed Eng. 2020;12(3).
20. Joy K. Optical and photoluminescence properties of nanostructured ZrO2:Tb thin films. Thin Solid Films. 2014;556:99-104.
21. Al-Bermany E, Mekhalif ATm, Banimuslem HA, Abdali K, Sabri MM. Effect of green synthesis bimetallic Ag@SiO_2 core–shell nanoparticles on absorption behavior and electrical properties of PVA-PEO nanocomposites for optoelectronic applications. Silicon. 2023;15(9):4095-4107.
22. Othman MS, Mishjil KA, Rashid HG, Chiad SS, Habubi NF, Al-Baidhany IA. Comparison of the structure, electronic, and optical behaviors of tin-doped CdO alloys and thin films. Journal of Materials Science: Materials in Electronics. 2020;31(11):9037-9043.
23. Abdali K, Al-Bermany E, Abass KH. Impact the silver nanoparticles on properties of new fabricated polyvinyl alcohol- polyacrylamide- polyacrylic acid nanocomposites films for optoelectronics and radiation pollution applications. Journal of Polymer Research. 2023;30(4).
24. Sakhil MD. Influence MgO Dopant on Structural and Optical Properties of Nanostructured CuO Thin Films. Neuroquantology. 2020;18(5):56-61.
25. Ghazai AJ, Abdulmunem OM, Qader KY, Chiad SS, Habubi NF. Investigation of some physical properties of Mn doped ZnS nano thin films. AIP Conference Proceedings: AIP Publishing; 2020. p. 020101.
26. Fadhl Abodood AA, Abdali K, Mousa Al-Ogaili AO, Al-Bermany E, Abass KH. Effect of Molar Concentration and Solvent Type on Linear and NLO Properties of Aurintricarboxylic (ATA) Organic Dye for Image Sensor and Optical Limiter Applications. International Journal of Nanoscience. 2023;22(02).
27. Khadayeir AA, Hassan ES, Mubarak TH, Chiad SS, Habubi NF, Dawood MO, et al. The effect of substrate temperature on the physical properties of copper oxide films. Journal of Physics: Conference Series. 2019;1294(2):022009.
28. Abdali K, Abass KH, Al-Bermany E, Al-robayi EM, Kadim AM. Morphological, Optical, Electrical Characterizations and Anti- Escherichia coli Bacterial Efficiency (AECBE) of PVA/PAAm/PEO Polymer Blend Doped with Silver NPs. Nano Biomed Eng. 2022;14(2).
29. Shaban ZM, Khlati JA, Khadayeir AA, Habubi NF, Chiad SS. Structural, Morphology and Optical properties of Ag-doped Nanostructured CdS thin films. Journal of Physics: Conference Series. 2021;1999(1):012063.
30. Aldulaimi NR, Al-Bermany E. Tuning the bandgap and absorption behaviour of the newly-fabricated Ultrahigh Molecular weight Polyethylene Oxide- Polyvinyl Alcohol/Graphene Oxide hybrid nanocomposites. Polym Polym Compos. 2022;30.
31. Chiad SS, Noor HA, Abdulmunem OM, Habubi NF, Jadan M, Addasi JS. Optical and Structural Performance of Nanostructured Te Thin Films by (Csp) With Various Thicknesses. Journal of Ovonic Research. 2020;16(1):35-40.
32. Ghazi RA, Al-Mayalee KH, Al-Bermany E, Hashim FS, Albermany AKJ. Impact of polymer molecular weights and graphene

nanosheets on fabricated PVA-PEG/GO nanocomposites: Morphology, sorption behavior and shielding application. AIMS Materials Science. 2022;9(4):584-603.
33. Ahmed NY. Effect of Boron on Structural, Optical Characterization of Nanostructured Fe2O3 thin Films. Neuroquantology. 2020;18(6):55-60.
34. Jabbar SA, Khalil SM, Abdulridha AR, Al-Bermany E, Karar A. Dielectric, AC Conductivity and Optical Characterizations of (PVA-PEG) Doped SrO Hybrid Nanocomposites. Key Eng Mater. 2022;936:83-92.
35. Salloom HT, Hadi EH, Habubi NF, Chiad SS, Jadan M, Addasi JS. Characterization of Silver Content Upon Properties of Nanostructured Nickel Oxide Thin Films. Digest Journal of Nanomaterials and Biostructures. 2020;15(4):1189-1195.
36. Salloom HT, Jasim RI, Habubi NF, Chiad SS, Jadan M, Addasi JS. Gas sensor using gold doped copper oxide nanostructured thin films as modified cladding fiber. Chinese Physics B. 2021;30(6):068505.
37. Hadi EH, Abbsa MA, Khadayeir AA, Abood ZM, Habubi NF, Chiad SS. Effects of Mn doping on the characterization of nanostructured TiO_2 thin films deposited via chemical spray pyrolysis method. Journal of Physics: Conference Series. 2020;1664(1):012069.
38. Chiad SS, Noor HA, Abdulmunem OM, Habubi NF. Optical and Structural properties of Ni-doped Co3O4Nanostructure Thin films Via CSPM. Journal of Physics: Conference Series. 2019;1362(1):012115.
39. Al-Abbas SS, Ghazi RA, Al-Bermany E, Sarheed AN, Albermany AKJ. Structure and absorption behaviour of PAAm-PVA-based nanocomposites reinforced using graphene. AIP Conference Proceedings: AIP Publishing; 2023.
40. Znaidi L, Soler Illia GJAA, Benyahia S, Sanchez C, Kanaev AV. Oriented ZnO thin films synthesis by sol–gel process for laser application. Thin Solid Films. 2003;428(1-2):257-262.